Forecasting the Fuel Consumption of Passenger Ships with a Combination of Shallow and Deep Learning

Ioannis Panapakidis [1,*], Vasiliki-Marianna Sourtzi [2] and Athanasios Dagoumas [2]

[1] Department of Electrical and Computer Engineering, University of Thessaly, 38221 Volos, Greece
[2] Energy & Environmental Policy Lab., School of Economics, Business & International Studies,
    University of Piraeus, 18532 Piraeus, Greece; vsourtzi@gmail.com (V.-M.S.); dagoumas@unipi.gr (A.D.)
[*] Correspondence: panap@teilar.gr; Tel.: +30-24210-74972

check for
updates

Abstract: An accurate fuel consumption prediction system for transportation units is the pillar that a more efficient fuel management can rely on. This in turn may eventually lead to cost and emission savings for the unit's owner. Numerous studies have been conducted for predicting the fuel usage in various means of transportation (i.e., airplanes, trucks, and vehicles). However, there is a limited number of researches that focus on passenger ships. These researches involve traditional machine learning models. There is a lack of literature on deep-learning-based forecasting models. The present paper serves as an initial study for exploring the potential of deep learning in day-ahead fuel consumption on a passenger ship. Firstly, a discussion is provided for the parameters that influence the fuel consumption. Secondly, the day-ahead fuel forecasting problem is formulated. To fully examine the influence of exogenous parameters on the consumption, various scenarios are formulated that differ in the types and number of inputs. The proposed forecasting model combines shallow and deep learning. Several machine learning and time series models were compared, and the results indicate the robustness of the proposed approach.

Keywords: deep learning; forecasting; fuel consumption; machine learning; passenger ships

1. Introduction

During the past years, it has been observed that due to the high demand of transporting goods via sea, there was a need of expanding the world's fleet [1]. That meant that at the same time the average fuel consumption has rapidly risen. This fact has significantly affected fuel prices, which have increased [2]. Nevertheless, such an increase in fuel prices was not enough to affect the afore-mentioned trend. This is partly justifiable, taking into consideration that due to globalization and the expansion of the fleet, there was also an increase in the income of the shipping companies. As time went by, both society and the shipping community started to become deeply concerned about the increase of the emissions that were produced as a result of commercial shipping [3]. The beginning of this concern was the "Kyoto Protocol", which introduced a series of measures that had to be urgently adopted in order to reduce the emissions of CO_2 and therefore restrict the global development of the greenhouse gases [4]. It was only in 2008 that shipping was included in the target of reducing the emissions of CO_2 as well as other greenhouse gases. As there was an expectation of an extreme growth of CO_2 in the future, shipping could no longer be a member of a non-regulation team in this matter. Further to the "Kyoto Protocol", the "Monitoring, Reporting, Verifying" (EU-MRV) regulation has been enforced in the shipping sector, suggesting that all the shipping companies and operators are obliged to monitor, report, and verify the ships' emissions and consequently to observe their daily fuel consumption [5]. At this point, it should be mentioned that most of the existing regulations are focused on the reduction of CO_2, as it is the predominant greenhouse gas. Moreover, a vessel's fuel

consumption and the production of emissions is a subject which has been analyzed, mostly based on container vessels. According to the International Maritime Organization (IMO), the vessels that produce highest emissions are those which are the most fuel consuming. Despite the fact that they do not represent a big part of the global fleet, container ships of 3000–5000 twenty-foot equivalent units (TEUs) and 5000–8000 TEUs and roll-on/roll-off passenger (Ro/Pax) vessels (i.e., ships carrying passengers and wheeled cargo) are the two most fuel-consuming categories. This has been repeatedly justified by their speed and the time they both need to stay in the port area [6].

The shipping industry plays a vital role in economic development, and it is recognized not only as the cornerstone of the world trade, as over 90% of the world's trade is carried by sea, but also as a low-cost transportation mean [6]. However, the growing demand of goods will lead to a rise of the world fleet—a fact that will result not only in an increase in global emissions from seaborne transportation but also more fossil fuel required for ships' operations [7]. It is well known that shipping-related activities mainly rely on fossil fuel consumption, a fact that has great impact not only to the environment but also on public health [8]. This fossil fuel utilization leads to the production of greenhouse gases (CO_2) but also nitrogen oxides (NOx) and sulfur oxides (SOx), which are related to human fatalities and environmental degradation [9]. According to the International Council on Clean Transportation for the period 1990–2007, it was observed that seaborne emissions increased from 585 to 1096 million tons [10]. According to [11], during 2008, the emissions generated from shipping amounted to 7.40 million tons. In addition to the above, it is noteworthy to mention that shipping emissions represent around 3.30% of the global anthropogenic emissions, and this percentage is expected to be increased by 2050 [11]. The shipping sector is the second-largest emitter of carbon dioxide compared to other transportation means [12]. From another point of view, it should be stated that bunkers have always been a key factor of shipping operations, as fossil fuels account for 50–60% of a company's operational running costs [13]. Thus, a potential increase in the price of oil will constitute a liability, as it will negatively affect the profitability of the shipping company or the operator. Therefore, the need for the development of a prediction tool for fuel consumption is clearly noted, as it would be considered not only a competitive advantage, but it can also contribute to the increase of company's revenues through sustained energy savings. This prediction tool can be used for achieving both optimization of the ship's operations and fuel efficiency [7].

It is a fact that few studies have been proposed so far on passenger ship fuel consumption prediction. Bal Beşikçi et al. developed an Artificial Neural Network (ANN) prediction model including seven input variables provided by a noon dataset (speed, trim, draft, weather conditions, quantity of the cargo) in conjunction with engine's revolutions per minute (RPM). This ANN-based model was used in a latter phase so that a decision support system for energy efficiency in real-time ship operations could be built. Furthermore, the prediction ANN model was compared to a Multiple Regression (MR) model, leading to the outcome that the former has greater prediction performance than the latter [14]. Petersen et al. modeled the fuel consumption for real-time conditions through the implementation of an ANN. More specifically, the factors that describe the dynamic state of the vessel (i.e., speed, trim, draft, propeller pitch, and engine's RPM) have been collected through sensors and were used as input variables to the model. The outcomes from this research provided that this model can obtain accurate results, and it can be used for a vessel's trim optimization [15]. Pedersen and Larsen presented in their study a neural network for a propulsion power predicting model by taking into account a vessel's noon report dataset, weather, and onboard measurement data. They concluded that the ANN model is more accurate compared to linear and non-linear models [16].

Taking into consideration all the above, it can be concluded that the developed models presented in these researches were mainly based on vessels' operational data collected either by a vessel's noon reports or through sensors on board. The literature review undertaken reveals that there are few studies on passenger ship fuel consumption. All those studies involve neural networks. More specifically, in [14], a neural network is compared with a regression model, while in [15] and [16], there is no comparison with other modeling approaches. While neural networks are a prominent forecasting

methodology for many applications, a comparison with other models enables the provision of more reliable conclusions regarding identifying more robust models for fuel consumption predictions. Since the passenger ship fuel consumption forecasting problem is a relatively under-examined research field, the authors of this study believe that as a first step to examine this problem, a comparison of models of different types and complexities should take place. Therefore, in the present paper, a novel forecasting hybrid model is proposed, combining shallow and deep learning. The model is compared with eight alternative models. This approach supports the conclusions drawn by the application of this hybrid model. The contribution of the paper concerns also the assessment of several cases of input data, compared to the literature, as studies [14–16] involve only one case of inputs. In the present paper, three different test cases of input combinations are formulated and applied. The scope is to investigate how different inputs influence the forecasting accuracy and determine which combination has the highest influence on the forecasting results. Another critical theme in forecasting studies is the evaluation framework. In [14], the evaluation takes into account two indices, while in [15,16], one indicator is used. In this paper, five indices are used, enhancing a more robust validation of the applied models. Thus, the present study contributes to the literature in the following ways: (a) it applies a novel model for passenger ship fuel consumption forecasting, which is compared with more alternative approaches compared to the literature; (b) more cases of inputs are used for the validation of the proposed methodology, compared to the literature; and (c) a more extended set of validation criteria is employed, compared to the literature. Examining passenger ship fuel consumption in a more detailed manner enables the provision of more robust conclusions on the validity of the proposed novel hybrid model.

This study focuses on the fuel consumption of Ro/Pax vessels, taking as a case study a specific vessel. This category has been chosen as it significantly raises the average port emissions, which does not significantly contribute to the national emissions inventory, but they are extremely important for the port's greater area emission management. In the present paper, a discussion on the factors that affect fuel consumption is provided. Next, the day-ahead fuel consumption forecasting problem is formulated and studied. A hybrid machine learning system that combines a Long Short-Term Memory (LSTM) Recurrent Neural Network (RNN) and an Elman Neural Network (ENN) is proposed for various cases that differ in terms of types and number of inputs [17]. This is due to fully evaluate the influence of exogenous parameters on fuel consumption. A comparison with other machine learning and time series models is performed, and superiority of the proposed model is observed.

2. Fuel Consumption

Fuel consumption is a principle exponential to a vessel's velocity, and it closely affects both the operational costs and the increase of greenhouse gas (GHG) emissions. Moreover, regarding fuel consumption, it should be taken into account that it is a complex variable due to its physical principles, which sometimes may lead to disputable and ambiguous results, a fact that makes a generalized explanation virtually impossible [18]. It should be noted that a vessel's total fuel consumption can be expressed as the sum of main and auxiliary engine consumptions while the vessel is at port and during its service at sea [19]. In the following, the types of fuels and the parameters which affect the fuel consumption are presented. Firstly, an important factor that must be taken into consideration is the type of fuel oil used onboard the vessels. Several studies have concluded that a vessel's energy efficiency and the fuel consumption are related to the type of fuel used. More specifically, according to [20], variations in fuel consumption are observed during the voyages due to fuel specifications (i.e., sulfur, water, ash quality, etc.). This can also be confirmed by the fact that engine manufacturers admit that the type of fuel in conjunction with operational practices may result in an increment in fuel consumption [21]. On the other hand, shipping companies and operators are forced to switch to bunkering fuel in order to meet regulation requirements. It should be noted that the ISO 8217 international standard classifies marine fuel oils into two distinct categories, distillate and residual fuel oils [22]. Heavy Fuel Oil (HFO) is an industrial fuel and is also known as a "refinery residual", as it is

incurred from refining process and more precisely from the distillation of crude oil [23]. HFO accounts for 80% of the global marine fuel oils used, and it is divided into three types regarding their sulfur content. In addition to the above, HFO is also classified, with regard to its viscosity, into HFO 180 and HFO 380 (i.e. 180 mm^2/s and 380 mm^2/s, respectively.) [24]. On the other hand, distillate marine fuel oils commonly used are Marine Gas Oil (MGO) and Marine Diesel Oil (MDO), and they are both classified as low in sulfur. Their main difference lies on the fact that MGO has a lower sulfur content and viscosity than MDO. It is essential to state here, that these distillate fuels are more expensive but lower in sulfur content than HFOs [25]. Moreover, it should be mentioned that unlike the low sulfur content, distillate marine fuels (MDO and MGO) have higher carbon contents—a fact that can be observed by the emission factors provided by the IMO [26]. Table 1 lists all the aforementioned information regarding the specifications of each fuel and the emissions factors.

Table 1. Fuel types, specifications, emission factors [27].

Fuel Types	Sulphur Content (mgS/kgfuel)	Carbon Content (kgC/kgfuel)	Emission Factors (t CO$_2$-eq/MWh)
HSFO 180	1–3.50%	≈0.85	3.114
HSFO 380	1–3.50%	≈0.86	3.116
LSFO 180	<0.50%	≈0.86	3.151
LSFO 380	<0.50%	≈0.86	3.151
ULSFO 180	<0.10%	≈0.86	3.151
ULSFO 380	<0.10%	≈0.86	3.151
MGO	0.10–1%	≈0.87	3.206
MDO	0.10–1.50%	≈0.87	3.206

From all the above, it is understood that the "bunkering switch" process to lower sulfur content fuel oil will have an impact on shipping companies due to the fact that low-sulfur bunkers are more expensive, which will result in additional costs and an increase of freight rates and ticket fares which will be passed on to customers [28]. Therefore, the implementation of low sulfur bunkering will affect short sea-shipping companies significantly, including companies owning Ro/Pax vessels, as operators will have to take a decision to either increase the ticket fare or to reduce daily itineraries. The "bunkering switch" process will increase the costs of a shipping company by around 80%. Another threat, that shipping companies may face is the fuel oil price volatility. In the case of a potential increase of fuel price, the cost will be passed on to the customer, resulting in the use of other, less expensive transportation modes [2]. Another issue is that in the case that the operator chooses to use low sulfur fuel oil onboard the vessels, this decision will lead to higher CO$_2$ emissions due to the fact that both MDO and MGO have higher carbon contents. Thus, the fuel switching process to fuels with low sulfur content may result in both additional costs and higher carbon emissions.

The prediction of fuel consumption plays an important role for the viability of a shipping company, and it is characterized by uncertainties, as it is clearly dependent on the ship's design, operational performance, and environmental conditions. The actual fuel consumption is monitored onboard the vessel through mass flow meters, which measure fuel oil usage both in main and auxiliary engines right after the arrival and the departure from the port. The ship design factors involve the main dimensions, cargo arrangement, propulsion system, engine specifications (main and auxiliary), propeller design, and hull/steel structure. The operational performance factors involve the performance itself at sea and at port, time in service at port, speed, draft, trim, displacement, hull performance, and drydocking. Finally, the environmental condition factors involve wind speed, wave height, and water and air temperature [29].

3. Fuel Consumption Forecasting

3.1. Test Case

This study is centered at a Ro/Pax vessel shipping from a port in Greece. This type of vessel is chosen, as in Greece, seaborne passenger transport is not only related to the country's economic development but also possesses a large share in the European market, representing 17% of the total passenger traffic in the EU [30]. The route under study is the Adriatic Route or, more precisely, the Patras–Igoumenitsa–Bari itinerary, as shown in Figure 1. According to [31], between 2016–2017, about 1,137,000 passengers have chosen this route, a fact that makes it one of the busiest maritime routes in Europe.
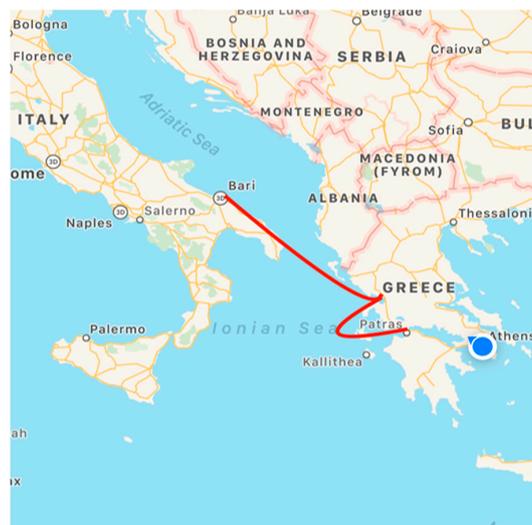
Figure 1. Route under study.

The Ro/Pax vessel is designed to transport passengers and vehicles (i.e., trucks, cars, etc.) and their design is characterized by complexity as they combine both transportation and hotel operation services in order to accommodate their passengers (i.e., restaurants, bars, cabins, etc.) [32]. The Ro/Pax vessels have three ship activities (cruising, maneuvering, and hotelling), and each of these produces an amount of emissions, as engine power is required to meet their energy needs [33]. This lead to the fact that apart from coastal shipping's vital role in the Greek economy, another important factor that must be studied is the energy consumption in Ro/Pax vessels, as they require more energy in order to meet not only the usual operations but also hoteling needs [34]. In the present paper, an existing Ro/Pax ferry is studied, namely the M/V ROPAX-NI, which has been performing a regular service on the Patras–Igoumenitsa–Bari route for more than 10 years. M/V ROPAX-NI is a high-speed vessel, and it is owned by a shipping company based in Greece. The ship owner provided all the necessary data. The vessel has a carrying capacity of 800 passengers and 140 trucks or 500 cars as cargo, and its guaranteed service speed is up to 23 knots. The vessel is operating on the route daily; more precisely, during the low season, from October until May, the vessel departs from the port of Patras every second day at 18:00, arriving at the ports of Igoumenitsa and Bari at 23:59 and 10:30 (the next day), respectively. From the port of Bari, the vessel departs at 20:30 and arrives at the ports of Igoumenitsa and Patras at 05:30 and 13:00 (the next day), respectively. It should be stated that the departure and arrival times correspond to Greek local time (GMT +2). Hence, it is observed that the voyage duration is 16 h and 30 min. During the high season, from June until September, the vessel also reaches the port of Corfu, departing from the port of Igoumenitsa but not on a daily basis. The voyage duration for this specific itinerary is 9 h and 30 min. Moreover, it should be mentioned that every two years, the vessel is out of service for a month in order to carry out its planned drydocking and maintenance. Apart from the geographical area where the ship is operating, another factor for choosing this case ship is that the

EU-MRV regulation has been implemented for this specific vessel from January 2018, and the company has developed a MRV monitoring plan in order to record and then verify all necessary data regarding emissions and fuel consumption. The minimum number of expected voyages falling under the scope of this regulation is 240 in accordance with ship's schedule.

3.2. Data Analysis

In this section, the integration of some operational, design, and environmental parameters and the fuel consumption will be explored and analyzed in order to find which factors have an impact on the vessel's fuel consumption. More precisely, a correlation analysis will be conducted in order to examine the aforementioned association. The potential relationship will be evaluated through the Pearson's correlation coefficient and scatter plots [35]. All the necessary data were derived from the vessel's 322 voyage reports, and the examined factors were selected based on the literature review. According to the discussion in Section 2, the total fuel consumption is affected by various parameters; thus, several factors by each category are considered in accordance with the data provided by the voyage reports. More specifically, from the ship design, the main engines' working hours and LSFO consumption are selected; from the operational performance, the average speed of the vessel, the distance, and the weight of the vessel (passengers, trucks, cars, etc.) are selected; and from the environmental conditions, the wind force in Beaufort Number (B.N.) is selected. In addition to the correlation between the aforementioned factors and the total fuel consumption, a correlation analysis between total fuel consumption and the fuel consumption of Low Sulfur Fuel Oil (LSFO), Marine Gas Oil (MGO), and High Sulfur Fuel Oil (HSFO) are also conducted, in order to perceive which of the previous fuels have greater impact on the total fuel consumption. Table 2 provides the findings after the conduction of a correlation analysis between the total fuel consumption and the aforementioned operational parameters.

Firstly, it is observed that there is a strong uphill linear correlational relationship between the total fuel consumption variable and the LSFO fuel consumption of the main engines, as the Pearson correlation coefficient was found 0.919. This result shows that those two variables are tightly associated, as the correlation coefficient value is very close to 1. This can be justified by the fact that during most of the voyage, the ship's main engines consume more LSFO, as it is operating in European navigational waters, where legislations obligate the operator to use fuel with low sulfur content. Moreover, positive correlations are also observed between the total fuel consumption and both HSFO and MGO fuel consumption variables with correlation coefficients of 0.373 and 0.165, respectively. This outcome can be justified by the fact that the HSFO is consumed by the main engines when the vessel is operating in international waters, while the MGO is consumed during the vessel's stay at port for only 5 h in conjunction with the fact that only auxiliary engines and boilers use this specific fuel. This observation can be explained by the fact that the MGO has a lower consumption, as it is used while the vessel is at port and only by auxiliary engines, which are operating for 5 h providing only the power required for covering the hotel operations. On the other hand, the LSFO, which has the highest fuel consumption, as it is consumed by the vessel's main engines, which are operating for 8 h in European waters, covering not only the hotel but also the propulsive demand. Although the HSFO is only consumed for 3.50 h during the vessel's passage through international waters, it has a stronger correlation with the total fuel consumption compared to MGO. This observation can be justified by the fact that the vessel has higher speed variations when it is sailing in high seas, resulting in higher engine rpm fluctuations and consequently in higher fuel consumption, a fact that is also confirmed by the findings of [36]. Additionally, the correlation coefficient between the examined variable and the distance is 0.886, and this fact points out a tight association as well. This can also be justified by the fact that the maximum value of the total fuel consumption (74.72 mton/h) is observed when the vessel reroutes for commercial reasons and calls at the port of Corfu, covering a distance of 400 miles whilst the scheduled itinerary was 318 miles (Patra–Igoumenitsa–Bari). Therefore, under this case, it is also confirmed that the fuel consumption is dependent on the distance covered.

Table 2. Correlation analysis of fuel consumption.

		TTL_FUEL_CONS	ME_LSFO_FUEL_CONS	ME_HSFO_FUEL_CONS	MGO_FUEL_CONS	AVERAGE_SPEED	MILES	WIND	WEIGHTS
TTL_FUEL_CONS	Pearson Correlation	1	0.919 **	0.373 **	0.165 **	−0.179 **	0.886 **	0.211 **	0.437 **
	Sig. (2-tailed)		0	0	0.003	0.001	0	0	0
	N	320	320	320	320	320	320	320	320
ME_LSFO_FUEL_CONS	Pearson Correlation	0.919 **	1	0.079	−0.089	−0.012	0.94 **	0.154 **	0.433 **
	Sig. (2-tailed)	0		0.158	0.112	0.836	0	0.006	0
	N	320	320	320	320	320	320	320	320
ME_HSFO_FUEL_CONS	Pearson Correlation	0.373 **	0.079	1	0.071	−0.303 **	0.078	0.297 **	OSS
	Sig. (2-tailed)	0	0.158		0.208	0	0.163	0	0.329
	N	320	320	320	320	320	320	320	320
MGO_FUEL_CONS	Pearson Correlation	0.165 **	−0.089	0.071	1	−0.256 **	−0.077	−0.022	−0.048
	Sig. (2-tailed)	0.003	0.112	0.208		0	0.169	0.691	0.389
	N	320	320	320	320	320	320	320	320
AVERAGE_SPEED	Pearson Correlation	−0.179 **	−0.012	−0.303 **	−0.256 **	1	−0.014	−0.447 **	0.204 **
	Sig. (2-tailed)	0.001	0.836	0	0		0.802	0	0
	N	320	320	320	320	320	320	320	320
MILES	Pearson Correlation	0.886 **	0.948 **	0.078	−0.077	−0.014	1	0.116 *	0.41 **
	Sig. (2-tailed)	0	0	0.163	0.169	0.802		0.038	0
		320	320	320	320	320	320	320	320
WIND	Pearson Correlation	0.211 **	0.154 **	0.297 **	−0.022	−0.447 **	0.116 *	1	−0.01
	Sig. (2-tailed)	0	0.006	0	0.691	0	0.038		0.856
	N	320	320	320	320	320	320	320	320
WEIGHTS	Pearson Correlation	0.437 **	0.433 **	0.055	−0.048	0.204 **	0.41 **	−0.01	1
	Sig. (2-tailed)	0	0	0.329	0.389	0	0	0.856	
	N	320	320	320	320	320	320	320	320

** Correlation is significant at the 0.01 level (2-tailed). * Correlation is significant at the 0.05 level (2-tailed).

Furthermore, the values of 0.211 and 0.437, which refer to the correlation coefficients between the fuel consumption and the variables of wind and weights, respectively, also indicate a positive linear relationship between the examined variables. At this point, it should be stated that the weight refers to the weight of cargo, the light ship, and the weight of bunkers. The dataset from voyage reports provided the number of passengers, trailer, trucks, campers, moto, buses, and cars, and in order to assess the total weight of the cargo, we used International Marine Organization's conversion factors for Ro/Pax load calculation [37]. The coefficient equal to 0.437 depicts that the vessel's weight has an impact on the fuel consumption; as the weight increases, the consumption rises as well. As it concerns the wind, the coefficient equal to 0.211 reveals that those variables are also associated and the fuel consumption is affected by the wind, but it also demonstrates that those two variables do not perform in the same way, as the weather conditions do not have a significant impact on fuel consumption. This can be justified by the fact that, on the one hand, the wind directions are not taken into account, and on the other, the impact of the wave effect cannot be estimated, which is considered the most important environmental factor. Last but not least, there is a negative correlation (i.e., –0.179) between the examined variable and the speed. This observation implies that there is not a tight association between these two variables while they move in opposite directions. The outcome of this statistical analysis indicates that the fuel consumption is tightly associated with the distance and the main engines' LSFO fuel consumption and consequently to the engine's operating hours. Moreover, the weight and the weather conditions (i.e., wind) also affect the fuel consumption. However, the results provide that there is a negative association between fuel consumption and speed. Figures 2 and 3 present the scatterplots between fuel consumption and Mechanical & Electrical (M&E) installation LSFO fuel consumption and distance, respectively.
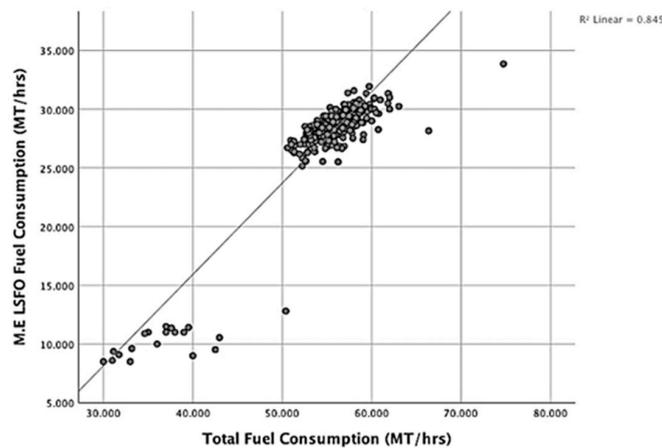

Figure 2. Scatterplot between fuel consumption and M&E LSFO fuel consumption.
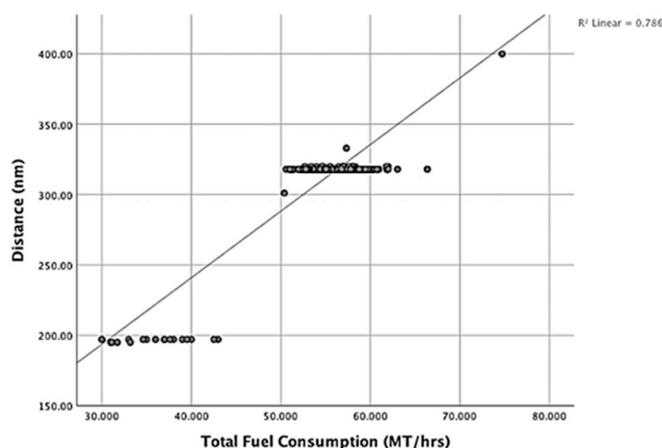

Figure 3. Scatterplot between fuel consumption and distance.

3.3. Scenarios

For the purpose of building an accurate prediction model, factors such as the vessel's speed, main engine working hours, fuel consumption, distance, weather conditions, and the weight of the vessel are taken into account. Therefore, previous theoretical and empirical findings will be applied. It is necessary to state that these factors should encompass ship design, environmental conditions, and operational performance. In order to feed, train, and validate a machine-learning-based prediction model, a significant amount of data is required. This research is mainly based on the ship's operational recorded data that are depicted in the voyage reports. This dataset, extracted from a MRV software, contains: the date, the time, the voyage number, departure and arrival ports, the vessel speed, the duration of the voyage, some hindcast weather data (B.N.), engine load, the vessel's loading conditions (cars, passengers, trailers, buses, motorcycles, and trucks), the voyage total fuel consumption, the voyage consumption per engine (main and auxiliary engines), boiler and fuel type (MGO, HFO, LSFO), the vessel's draft (trim, aft, fore), and CO_2 emissions. The crew onboard feed this voyage report every 24 h with all necessary data provided by the measurement instruments during the voyage and vessel's stay at port. This study was carried out by taking into account 322 electronic operational reports which are referred to the period from 1st January 2018 until 31st October 2018 for one vessel that is operating in the Adriatic route.

In general, a forecasting task can be formulated through a time-series-based nonlinear discrete-time dynamical model:

$$L(t+1) = f(L(t), \ldots, L(t-m+1); X) \tag{1}$$

where $L(t)$ is the consumption at time t, and m is the order of the system and is a vector that contains external variables such as average speed of the vessel, wind force, and others. Hence, the forecasting task is to propagate historical consumption values in a future time interval. The value of m is defined through mathematical analysis or it is determined by expert knowledge. The elements of X are problem specific. In the present study, time t corresponds to a day. A critical parameter during the construction of a model is the proper selection of the number and types of inputs. Historical consumption values are always a candidate input. Other variables can be selected either by correlation analysis or based on the related literature. The order of the system m will be defined by an autocorrelation analysis. Figure 4 displays the Pearson correlation coefficient curve between fuel consumption's current values and its preceding values of 30 days. Values above 0.90 are highly correlated and can serve as inputs. However, the results reveal the absence of strong autocorrelation between fuel consumption values for the aforementioned lags, a fact that may lead to low prediction accuracy. Let d be the indicator denoting the target day. The consumption of days $d-1$ and $d-8$ are selected since they display the highest correlation. In order to fully assess the variation of types and number of inputs to the model's prediction accuracy, three case studies are formulated and examined:

- Case Study #1: The inputs include only historical values of the target variable. More specifically, past consumption values $L(d-1)$ and $L(d-8)$ are the inputs of the prediction model. No external variables are considered.
- Case Study #2: Only external variables are regarded, i.e., the average vessel's speed, wind force, the number of passengers, main engine hours, total consumption of LSFO, and the distance. It is necessary to point out that the number of passengers is taken into account as it has an impact on the vessel's weight and consequently on the total fuel consumption. Therefore, the following input neurons are regarded:

  -       Input 1: Average Speed of the vessel at the day $d-1$
  -       Input 2: Average Speed of the vessel at the day d
  -       Input 3: Wind Force at the day $d-1$
  -       Input 4: Wind Force at the day d
  -       Input 5: Number of passengers at the day $d-1$

-     Input 6: Number of passengers at the day d
-     Input 7: Main engine hours and total consumption LSFO at the day $d - 1$
-     Input 8: Main engine hours and total consumption LSFO at the day d
-     Input 9: Distance at the day $d - 1$
-     Input 10: Distance at the day d

- Case Study #3: This case study combines the previous cases. The number of inputs is 12.
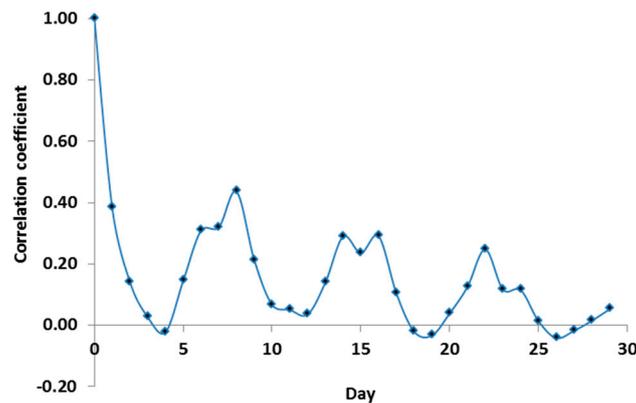

Figure 4. Correlation coefficient curve.

3.4. Model

LSTM is an RNN architecture which was designed to approach and model time sequences and their large range of dependencies more accurately than other types of RNN. The concept of RNNs is that they utilize sequential information. In a conventional Feed-Forward Neural Network (FFNN), all inputs and outputs are independent of one another. The recurrent operation lies on the fact that an RNN performs the same process for each element of a sequence, where the output depends on the previous calculations. RNNs have a memory that captures information about what it has been calculated so far, i.e., in the specific time instance. This means that they are able to explore temporal relationships. Figure 5 presents an RNN that unfolds into a full network. The unfolding represents the neural network as a full sequence of simple structure hidden units. Let $x = \{x_1, x_2, \ldots, x_t\}$ be a vector representing a time series; x_t represents the input at time instant t. The RNN computes the hidden state sequences $h = \{h_1, h_2, \ldots, h_t\}$, where h_t represents the hidden state at the time instant t and actually is the memory of the network. The latter is computed based on the previous hidden state h_{t-1} and the current input x_t :

$$h_t = f(W_{hx}x_t + W_{hh}h_{t-1} + b_h) \tag{2}$$

where W_{hx} and W_{hh} refer to the input/hidden and hidden/hidden weight matrices, respectively, and b_h is the bias of the hidden layer. The activation function f is usually non-linear, such as a rectified linear unit or sigmoid tanh. The output y_t at time instant t is expressed as:

$$y_t = g(W_{hy}h_t + b_y) \tag{3}$$

where g is the activation function of the output layer, W_{hy} is the hidden/output weight matrix, and b_y is the bias of the output layer. The training process of an RNN is similar to the one of FFNN; the backpropagation algorithm is used but in a modified version, i.e., the gradient of each output depends not only on the calculations for the current time instance, but also on the previous time instances [38]. The structure of the LSTM is given in Figure 6. LSTMs do not display substantial difference in their architecture compared to RNNs. However, they use a different function to calculate the hidden state. The memory in the LSTM is called cell and receives as inputs h_{t-1} and x_t. Internally,

the cell defines what will be kept and erased from the memory. Next, they combine the previous state, the current memory, and the input.
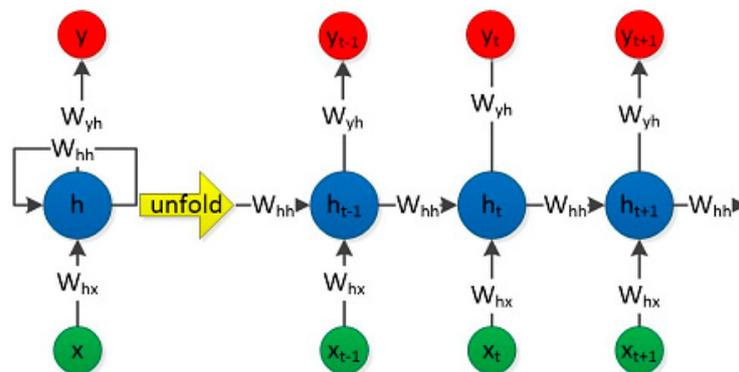

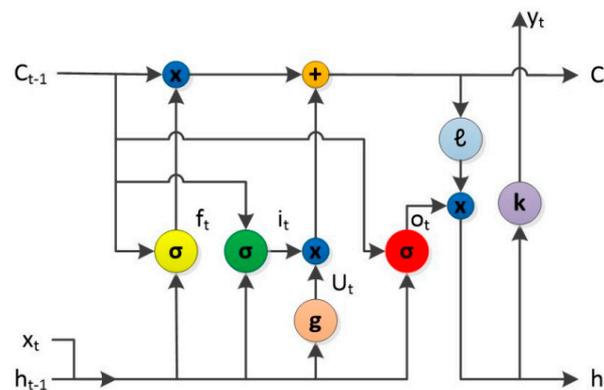**Figure 5.** Unfolding of Recurrent Neural Network (RNN) [38].

Figure 6. Long Short-Term Memory (LSTM) structure [38].

A cell block is composed of an input gate i, a forget gate f, a self-connected memory cell C, and the output gate y. They are called gates because the sigmoid function compresses the values of these vectors between 0 and 1, and by multiplying them by another vector, it is feasible to control to what degree this vector will affect the output. The entrance gate determines what amount of the new calculated state for the current input is required to pass. The input gate controls the entry of the activations to the memory cell. The forget gate defines what amount of the previous state will pass, and finally, the output gate defines the amount of the internal state required to exit the network. All gates have the same dimensions, i.e., they have the same size of hidden states. The term g denotes the candidate hidden state which is calculated using the input of the current time instance and the hidden state of the previous time instance. The memory C is a combination of the internal memory of the previous time instance multiplied by the forget gate and the new hidden state g multiplied by the input gate. First of all, the forget gate is applied in order to decode which information will be kept or dismissed. The output of the forget gate at time instance t and f receives values among 0 and 1 and is calculated as:

$$f_t = \sigma(W_{fx}x_t + W_{fh}h_{t-1} + W_{fc}C_{t-1} + b_f) \tag{4}$$

where σ is the sigmoid activation function of the forget gate; W_{fx}, W_{fh}, and W_{fc} are the forget/input, forget-hidden, and forget/memory weight matrices, respectively; C_{t-1} is the memory state at instance $t-1$; and b_f is the bias of the forget gate. The output of the input gate layer i is given by:

$$i_t = \sigma(W_{ix}x_t + W_{ih}h_{t-1} + W_{ic}C_{t-1} + b_i) \tag{5}$$

where W_{ix}, W_{ih}, and W_{ie} are the input gate/input, input gate/hidden, and input gate/memory weight matrices, respectively, and b_i is the bias of the input gate. In the input gate, it is decided which information will be kept or not. A vector U_i is formed to store the new candidate values to be added to the new cell state:

$$U_t = \sigma(W_{cx}x_t + W_{ch}h_{t-1} + b_c) \tag{6}$$

where W_{cx} and W_{ch} are the cell state/input and cell state/hidden weight matrices, respectively, and b_c is the bias of the cell state. The new cell state C_t is obtained combining the values of C_{t-1}, U_t, i_t, and f_t:

$$C_t = U_t i_t + C_{t-1} f_t \tag{7}$$

A sigmoid layer is used as the output gate to filter provide the cell state o_t:

$$o_t = \sigma(W_{ox}x_t + W_{oh}h_{t-1} + W_{oc}C_{t-1} + b_o) \tag{8}$$

where W_{ox}, W_{oh}, and W_{oc} are the output gate/input, output gate/hidden, and output gate/memory weight matrices, respectively, and b_o is the bias of the output gate. Next, a cell output sigmoid activation function l is applied over the cell state:

$$h_t = o_t l(C_t) \tag{9}$$

The output of the memory block y_t is calculated via the following equation:

$$y_t = k(W_{yh}h_t + b_y) \tag{10}$$

where k is the output activation function, W_{yh} is the output/hidden weight matrix, and b_y is the bias of the output.

The operation of the proposed model relies on the serial operation of LSTM and the ENN. The structure of the model is depicted in Figure 7. First, the LSTM is executed and provides an initial forecast. This forecast is inserted to the ENN, together with the rest of inputs per case. The output of the ENN is the final forecast of the fuel consumption. The ENN uses one additional input compared to the LSTM which is the output of the latter.
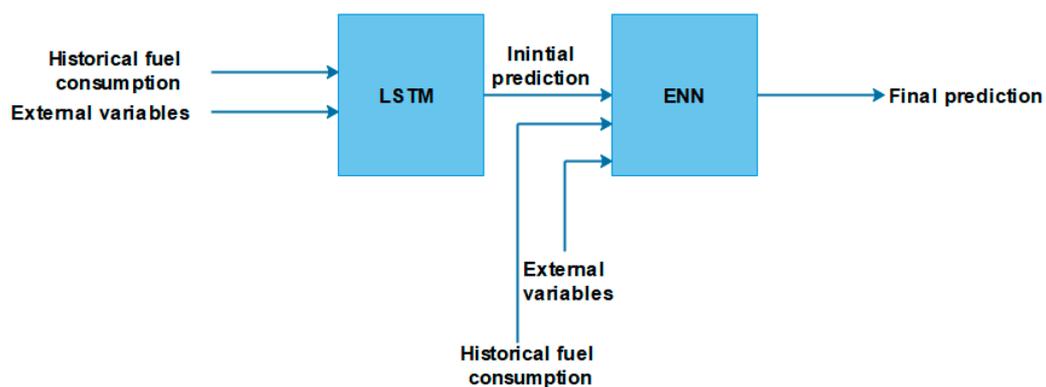

Figure 7. Schematic representation of the proposed model.

4. Results

The scope of the analysis of the paper is to forecast the total ship fuel demand (LSFO) in a day-ahead time frame using various inputs combinations. The examined time period refers to 02/01/2018–14/11/2018, i.e., a total of 322 days. Figure 8 presents the fuel consumption time series. The period 02/01/2018–12/09/2018 serves as a training set, and the period 13/09/2018–14/11/2018 as test set. The training set covers almost 80% of the total data, and the remaining 20% refer to the test set. The training set is used to derive the optimal parameters of the models (i.e., structure, number of

neurons, number of epochs, etc.) while the test set is employed for the models' comparison. It can be noticed that there are several spikes in the time series, a fact that makes fuel demand forecasting a challenging task.
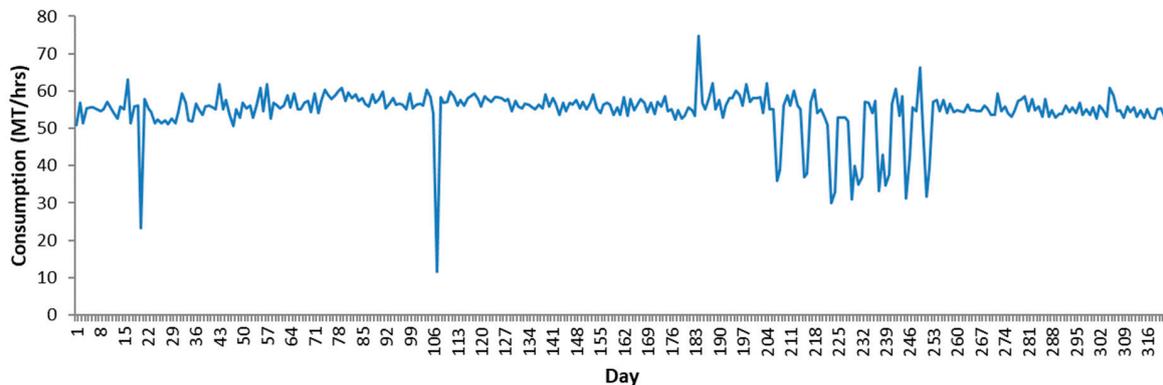
Figure 8. Fuel consumption time series.

The prediction accuracy will be evaluated with a set of mathematical indicators. Let P_m^a and P_m^τ be the actual and predicted fuel demand of the *m*-th day of the test set, $m = 1,2, \ldots ,$M and $M = 65$, respectively. The Absolute Error (AE) is defined as [39]:

$$\mathrm{AE} = \sum_{m=1}^{M} \left| P_m^a - P_m^f \right| \tag{11}$$

The Mean Absolute Error (MAE) refers to the sum all AEs [39]:

$$\mathrm{MAE} = \frac{1}{M} \sum_{m=1}^{M} \left| P_m^a - P_m^f \right| \tag{12}$$

The Mean Absolute Percentage Error (MAPE) is given by [39]:

$$\mathrm{MAPE} = \frac{1}{M} \sum_{m=1}^{M} \frac{\left| P_m^a - P_m^f \right|}{P_m^a} \times 100 \tag{13}$$

The Root Mean Squared Error (RMSE), is expressed as [39]:

$$\mathrm{RMSE} = \frac{1}{M} \sqrt{\sum_{m=1}^{M} \left(P_m^a - P_m^f \right)^2} \tag{14}$$

The Mean Absolute Range Normalized Error (MARNE) is the absolute difference between the actual and forecast natural gas demand, normalized to the maximum fuel demand [40]:

$$\mathrm{MARNE} = \frac{1}{M} \sum_{m=1}^{M} \frac{\left| P_m^a - P_m^f \right|}{\max(P_m^a)} \times 100 \tag{15}$$

To fully validate the LSTM model, a comparison takes place with Radial Basis Function Neural Network (RBFNN) [41], General Regression Neural Network (GRNN) [42], Elman Neural Network (ENN) [43], Support Vector Regression (SVR) [44], Group Method of Data Handling (GMDH)-based neural network [45], Relevant Vector Machine (RVM) [46], Feed-Forward Neural Network (FFNN) [47], and Multiple Regression Model (MRM) [48]. Regarding the MRM, a linear model is assumed. Not only does it assess the effect of two or more independent variables to the dependent variable, but it also

predicts the value of the dependent variable taking into account the values of predictors, and hence, its equation is defined by the following formula:

$$y = a + b_1 x_1 + b_2 x_2 + \ldots + b_n x_n + \varepsilon \tag{16}$$

where y is the response variable, $x_1, x_2, \ldots, x_n$ are the explanatory or independent variables, $a, b_1, b_2, \ldots, b_n$ are the regression coefficients, and ε is the error term. In order to model the relationship between an independent variable and a predictor by applying multiple regression analysis, the following assumptions must be tested [49]:

- The dependent and at least two predictor variables must be continuous.
- Linearity between the dependent variable with each one of predictors. The independent variable must be expressed as a linear function of independent variables.
- The difference between the predicted and the actual values (residuals) must follow the Gaussian distribution.
- Absence of multicollinearity, a fact which underlies that regressors (independent variables) must not be tightly correlated to each other.
- Absence of autocorrelation, a fact which provides that the residuals must be independent from each other. Therefore, the observations must be independent from their past values.
- The residuals must be homoscedastic (constant variance of errors).

In the case that one of the aforementioned assumptions are not met, then the implications of the violation may lead to invalid or misleading results, and therefore the model must be adjusted. However, not all violations have the same impact on the analysis. More precisely, a linearity violation is critical, and it results in biased predictions, while a violation in the independence of residuals has an impact only on standard errors. Additionally, a violation in homoscedasticity negatively influences the standard errors and the statistical significance [48]. The statistical procedure of the least square method will be applied in order to reduce the squares of residuals occurred by the results. Another aspect that holds a crucial role is the goodness of fit in conjunction with the statistical significance, which will reveal whether the regression model adequately describes the set of observations.

In order to perform the multiple regression analysis, the original variables are converted into standardized values (z-scores). The overall MRM accuracy and how well the regression line fits will be determined by the coefficient of determination (R^2), and its values must range between 0 and 1, where values closer to 1 indicate a perfect fit. Another aspect that must be evaluated is the significance of the model, which will be determined by the p-values by taking into consideration that the level of significance is $a = 0.05$. Referring to Table 2, it is observed that the predictor variables "Main Engine & Total LSFO Consumption" and "Miles" are perfectly correlated with $r = 0.998$, a fact which indicates the occurrence of multicollinearity in the regression model. Hence, the independent variable "Miles" is omitted from the MR analysis. Furthermore, a stepwise regression procedure will also be applied in order to identify which predictor variables add variability to the model resulting in the increase of R^2. As a result, the multiple regression analysis will be divided into two categories concerning the selection process (enter and stepwise) by which the predictor variables are entered in the equation. Utilizing the enter method selection process, all predictor variables are entered in the equation simultaneously, and the results from the regression analysis performed are depicted in Table 3.

Table 3. Model summary utilizing the enter method.

Model	R	R^2	Adjusted R^2	Std. Error of the Estimate	Durbin–Watson
1	0.911	0.831	0.819	1.16219	2.118

It is observed that $R^2 = 0.831$, a fact that shows that the relationship between the dependent and the predictor variables is strong enough, so that the 83% of the variation of the total fuel consumption

are linearly explained by the predefined independent variables. The remaining 17% of the variation in total fuel consumption can be explained by other factors, such as the vessel's total resistance, hull roughness, etc. Another factor that must be taken into account is the Adjusted R^2, which is not much lower than R^2, a fact that shows that the regression model can be generalized to the population. Hence, the 81% of total variance of the response variable can be explained by the model. Moreover, from the Durbin–Watson (DW) value DW $= 2.118$, it is assumed that there is no linear autocorrelation in residuals, as it falls within the range of 1.50 and 2.50. The Standard Error (SE) represents the regression error. In our case, SE $= 1.16$, i.e., 1.16% of variance in the Total Fuel Consumption cannot be explained by the regression model. Therefore, it is understood that the SE is not high enough, leading to the fact that the values are well-fitted to the regression line.

From the ANOVA results in Table 4, we may examine the *p*-value in order to evaluate the significance of the regression model and whether the predictor values contribute significantly to the prediction of the total fuel consumption values. It is observed that the model's *p*-value accounts for 0.000 while the level of significance is $a = 0.05$; hence, the *p*-value is much lower than the level of significance. As a result, it is proved that the developed model is significant.

Table 4. ANOVA results.

	Model	Sum of Squares	df	Mean Square	F	Sig.
	Regression	397.160	4	99.290	73.510	0.000
1	Residual	81.042	60	1.351		
	Total	478.202	64			

Table 5 presents the results of the regression analysis utilizing the enter method. It can be noticed that the contribution of the independent variables to the model is indicated by the column "Sig." More specifically, from the predictors' *p*-values, it is observed that almost all independent variables significantly contribute to the regression model. However, only the wind variable with a *p*-value of 0.424 does not contribute. Moreover, when examining the Variation Inflation Factor (VIF), the absence of multicollinearity is noted, as VIF only denotes the occurrence of multicollinearity in the model when the it ranges between 5 and 10.

Table 5. Regression analysis outcomes using the enter method.

	Coefficients [a]							
Model	Unstandardized Coefficients		Standardized Coefficients	*t*	Sig.	Collinearity Statistics	
	B	Std. Error	Beta			Tolerance	VIF
(Constant)	55.217	0.144		383.043	0		
Zscore (ME_LSFO_fc)	1.871	0.179	0.684	10.466	0	0.661	1.514
1 Zscore (avg_speed)	−0.884	0.195	−0.323	−4.538	0	0.556	1.799
Zscore (wind)	0.179	0.223	0.066	0.805	0.424	0.425	2.351
Zscore (pax)	0.475	0.149	0.174	3.178	0.002	0.944	1.059

[a] Predictors: (Constant), Zscore(ME_LSFO_fc).

Furthermore, the B column is used in order to develop our regression model, as the values in the column are replacing the coefficients. These coefficients represent the association between the total fuel consumption and the independent variables. However, from Table 5, it is noted that the predictor "Average Speed" has a negative coefficient, fact that indicates the negative association between this variable and the independent variable. This observation can be justified by the fact that the speed reduction can lead to higher fuel consumption due to the increase in the hull resistance and consequently to an increment in Effective Horsepower [50]. Hence, the MRM has the following form:

$$y = 55.217 + 1.871 \times \text{ME LSFO} + 0.179 \times \text{Wind} - 0.884 \times \text{Speed} + 0.475 \times \text{Pax} \tag{17}$$

Using the stepwise selection process to identify all the explanatory variables that significantly influence the dependent variable, the model summary is derived and presented in Table 6. The results from the regression analysis indicate that the model with the highest R^2 (0.829) is the third one, which incorporates the variables average speed, M&E LSFO fuel consumption, and number of passengers, while the variable wind is omitted from the regression analysis, as it does not significantly contribute to the model's ability to predict the fuel consumption. This observation was also confirmed when applying the enter method.

Table 6. Model summary utilizing the stepwise method.

Model	R	R^2	Adjusted R^2	Std. Error of the Estimate	Durbin–Watson
1	0.838 [a]	0.701	0.697	1.50545	
2	0.895 [b]	0.800	0.794	1.24079	
3	0.910 [c]	0.829	0.820	1.15883	2.065

[a] Predictors: (Constant), Zscore(ME_LSFO_fc). [b] Predictors: (Constant), Zscore(ME_LSFO_fc), Zscore(avg_speed). [c] Predictors: (Constant), Zscore(ME_LSFO_fc), Zscore(avg_speed), Zscore(Pax).

The coefficients and the variables used in the three regression models are illustrated in Table 7. Furthermore, it is also denoted that only the variables with a *p*-value of more than 0.05 were entered in the model. More precisely, from the t-values, it is observed that the strongest predictor is the main engine hours and LSFO total consumption, as fuel consumption is tightly associated with the main engine's working hours in conjunction with the LSFO fuel usage. It is denoted that also in the stepwise process, the average speed has a negative association with the dependent variable. The results also revealed the absence of multicollinearity in the regression model.

Table 7. Regression analysis outcomes from the stepwise method.

		Coefficients [a]						
	Model	Unstandardized Coefficients		Standardized Coefficients	t	Sig.	Collinearity Statistics	
		B	Std. Error	Beta			Tolerance	VIF
1	(Constant)	55.217	0.187		295.707	0		
	Zscore(ME_LSFO_fc)	2.289	0.188	0.838	12.166	0	1	1
2	(Constant)	55.217	0.154		358.780	0		
	Zscore(ME_LSFO_fc)	2.042	0.161	0.747	12.650	0	0.923	1.083
	Zscore(avg_speed)	−0.895	0.161	−0.327	−5.545	0	0.923	1.083
3	(Constant)	55.217	0.144		384.154	0		
	Zscore(ME_LSFO_fc)	1.943	0.154	0.711	12.628	0	0.886	1.129
	Zscore(avg_speed)	−0.981	0.153	−0.359	−6.404	0	0.895	1.118
	Zscore(pax)	0.473	0.149	0.173	3.175	0.002	0.945	1.059

[a] Predictors: (Constant), Zscore(ME_LSFO_fc).

From the interpretation of the scatter plot in Figure 9, the relationship between the actual and predicted values of the fuel consumption is depicted (322 observations). It should be stated that the x-axis shows the fuel consumption actual values, while the y-axis represents the predicted values of the fuel consumption. A positive slope is clearly observed, a fact that reflects the uphill positive relationship. Nevertheless, it should be stated that some outliers may be identified.

The basic model parameters derived from the training process of each model are the following: For the RBF and GRNN, the spread of the radial basis function is set to 1; for the ENN, the number of hidden layer neurons is set to 10; for the SVR, the type of kernel is linear and the kernel scale parameter is set to 1; for the GMDH, the number of layers is set to 4; the number of neurons in each layer is set to 14, and alpha parameter is set to 0.5; for the RVM, the kernel width is set to 5 and the likelihood is Gaussian type; for the FFNN, the number of hidden layers is set to 1, the activation function in both the hidden and output layer is hyperbolic tangent sigmoid, the maximum number of epochs is set to

1000, and the network is trained with the Bayesian regulation back-propagation algorithm [51]; and for the LSTM, the number of epochs is set to 25, and the initial learning rate is set to 0.005.
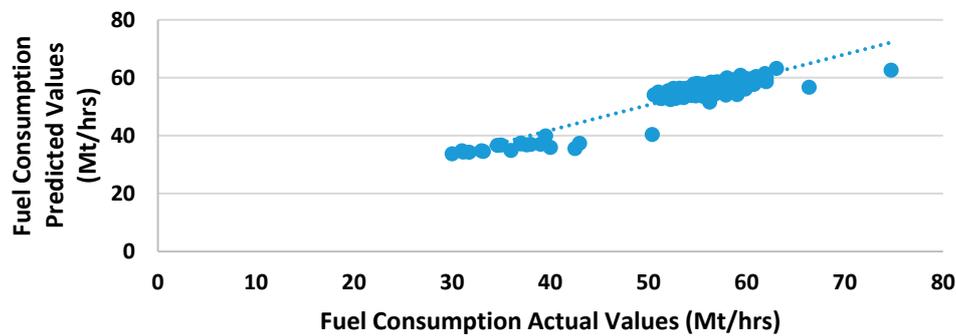

Figure 9. Scatter plot of actual values and predicted values.

The scores of the models on the error indicators are presented in Table 8, Table 9, and Table 10 for Case Study #1, Case Study #2, and Case Study #3, respectively. Instead of utilizing one error metric, a set of metrics leads to more accurate comparisons of the models. An ideal model should lead to lower errors in most, if not all, of the cases. MAE and RMSE measure the difference between the forecast and the actual value. MAPE and MARNE are percentage indicators. MARNE provides a solution to the inherent limitation of MAPE when zero or extremely low values are present in the data set. In this case, MAPE would be very high, a fact that does not provide reliable indication on the forecasting performance.

Table 8. Models comparison for Case Study #1.

Model	MAE (mton/h)	RMSE (mton/h)	MAPE (%)	MARNE (%)
ENN	1.538	2.069	2.753	2.532
FFNN	1.404	2.032	2.514	2.311
GMDH	1.595	2.324	2.851	2.627
GRNN	2.677	4.000	4.884	4.408
RBF	2.979	4.102	5.435	4.905
RVM	1.547	1.943	2.787	2.546
SVR	1.697	2.190	3.092	2.794
LSTM-ENN	1.398	1.936	2.506	2.301

Table 9. Models comparison for Case Study #2.

| Model	MAE (mton/h)	RMSE (mton /h)	MAPE (%)	MARNE (%)
ENN	1.268	1.532	2.322	2.089
FFNN	1.327	1.628	2.441	2.185
GMDH	1.670	2.002	3.072	2.750
GRNN	2.673	3.226	4.877	4.402
RBF	3.957	4.539	7.243	6.516
RVM	1.723	2.010	3.143	2.836
SVR	1.351	1.719	2.472	2.225
LSTM-ENN	1.250	1.715	2.281	2.057
MRM	4.224	5.424	7.672	6.995

Table 10. Models comparison for Case Study #3.

Model	MAE (mton /h)	RMSE (mton /h)	MAPE (%)	MARNE (%)
ENN	1.304	1.675	2.379	2.147
FFNN	1.274	1.632	2.319	2.097
GMDH	1.218	1.628	2.345	2.194
GRNN	2.682	3.228	4.892	4.417
RBF	3.867	4.446	7.080	6.367
RVM	1.935	2.198	3.543	3.186
SVR	1.229	1.607	2.218	2.024
LSTM-ENN	1.197	1.568	2.177	1.971

According to the above regression analysis, the MRM is applicable only for Test Case #2. It can be observed that in all examined cases the proposed LSTM-ENN model results in lower errors. According to Table 8, the FFNN and the ENN display robust performance. Highest errors correspond to GRRN and RBF. GMDH and RVM leads to comparable performance. The inputs of Test Case #2 appear more promising for the fuel demand forecasting problem under study. In Table 9, it is shown that all errors values are lower compared to Test Case #1 apart from GMDH. The latter is more robust in Test Case #1, where a reduced set of inputs is used. Moreover, no considerable differences are noticed in the operation of GRNN when MAPE indicator is used. When considering MAE and RMSE, which measure deviations from the target value, the difference is more visible. As in Test Case #1, ENN and FFNN are next in the comparison ranking after the LSTM-ENN model. SVR is the 4th model that leads to MAPE below 3%. GMDH comes next in the competition. RBF and MRM lead to MAPE values above 7%. For most of the models, Test Case #3 leads to lower errors. For instance, the LSTM-ENN model manages to provide even better accuracy. Moreover, ENN and FFNN score MAPE values below 2.50%. On the contrary, RVM increases its error. As in the previous cases, the RBF neural network corresponds to poor prediction performance, and hence, it is not recommended for the problem under study.

The findings in Tables 8 and 9 revealed that the fuel consumption is more related to exogenous factors rather using only its preceding values. This is also evident from the results of the correlation analysis presented in Figure 4. The specific time series does not display strong autocorrelation with its preceding values. Moreover, the forecasting models are also dependent on the previous day values of the variables used. Therefore, a model can provide the fuel consumption prediction for the day ahead when several parameters are known; consequently, this can also lead to the prediction of ship-generated emissions. In addition, the total fuel consumption can be expressed as a nonlinear function of operational, design, and environmental parameters (i.e., average vessel speed, wind force, number of passengers, distance, and ME Hours and Total Consumption of LSFO).

The AE distributions for Test Case #1, Test Case #2, and Test Case #3 are illustrated in Figure 10, Figure 11, and Figure 12, respectively. The selected bin in the horizontal axis is set to 2 mtonMt/h. The number of instances per bin is also shown. Recall that the test set is composed of 65 days. According to the figures, the optimal forecaster refers to the cases that most instances are within the [0,2] range. In some models, i.e., RBF, there are instances above 10 Mt/h; these cases refer to forecasting failure. This is also the case with the MRM. It provides seven forecasts where the AE exceeds the 10 Mt/h upper threshold.
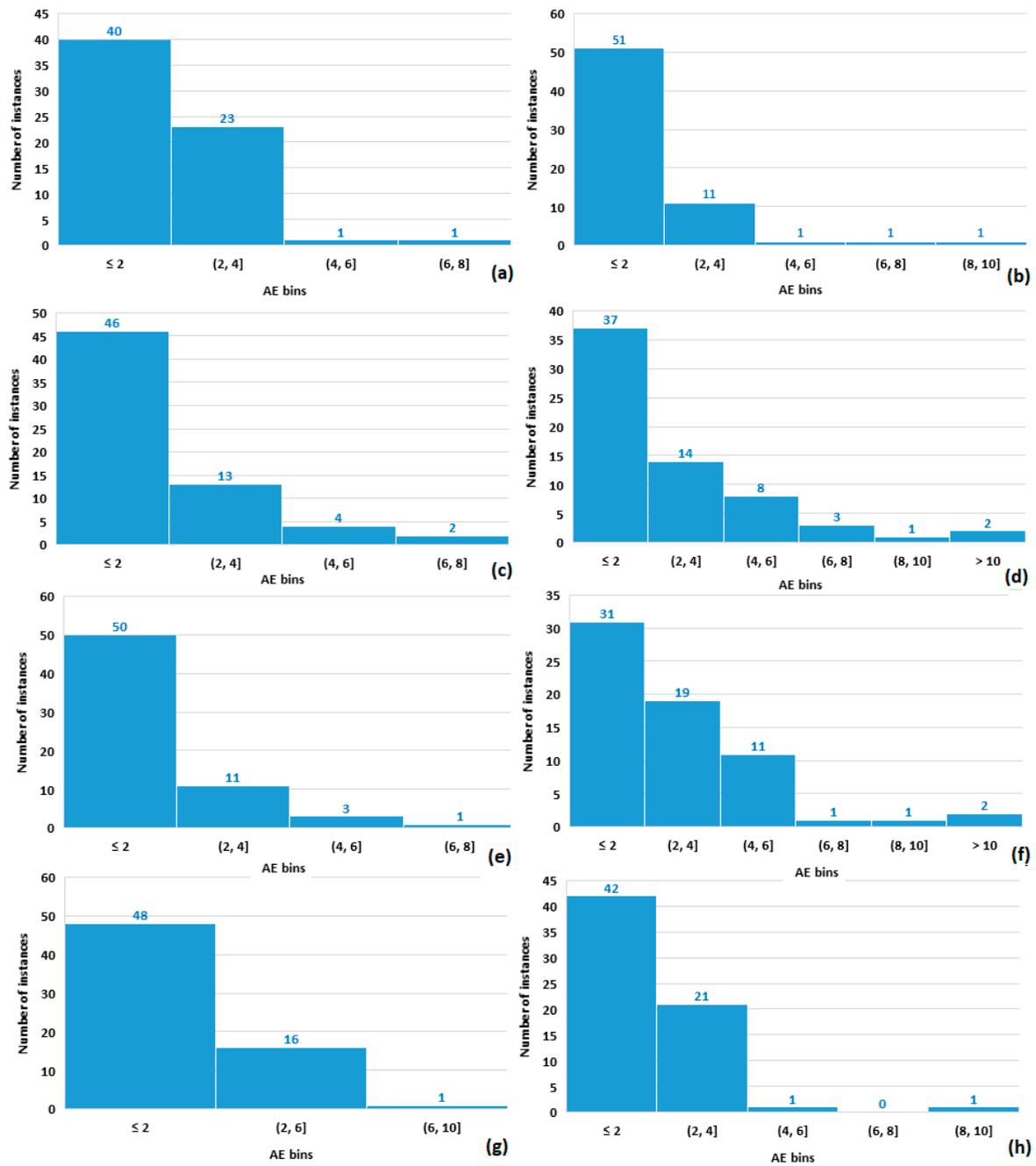
Figure 10. Absolute Error (AE) distribution for (**a**) Elman Neural Network—ENN, (**b**) Feed-Forward Neural Network—FFNN, (**c**) Group Method of Data Handling—GMDH, (**d**) General Regression Neural Network—GRNN, (**e**) LSTM-ENN, (**f**) Radial Basis Function—RBF, (**g**) Relevant Vector Machine—RVM, and (**h**) Support Vector Regression—SVR for Test Case #1.
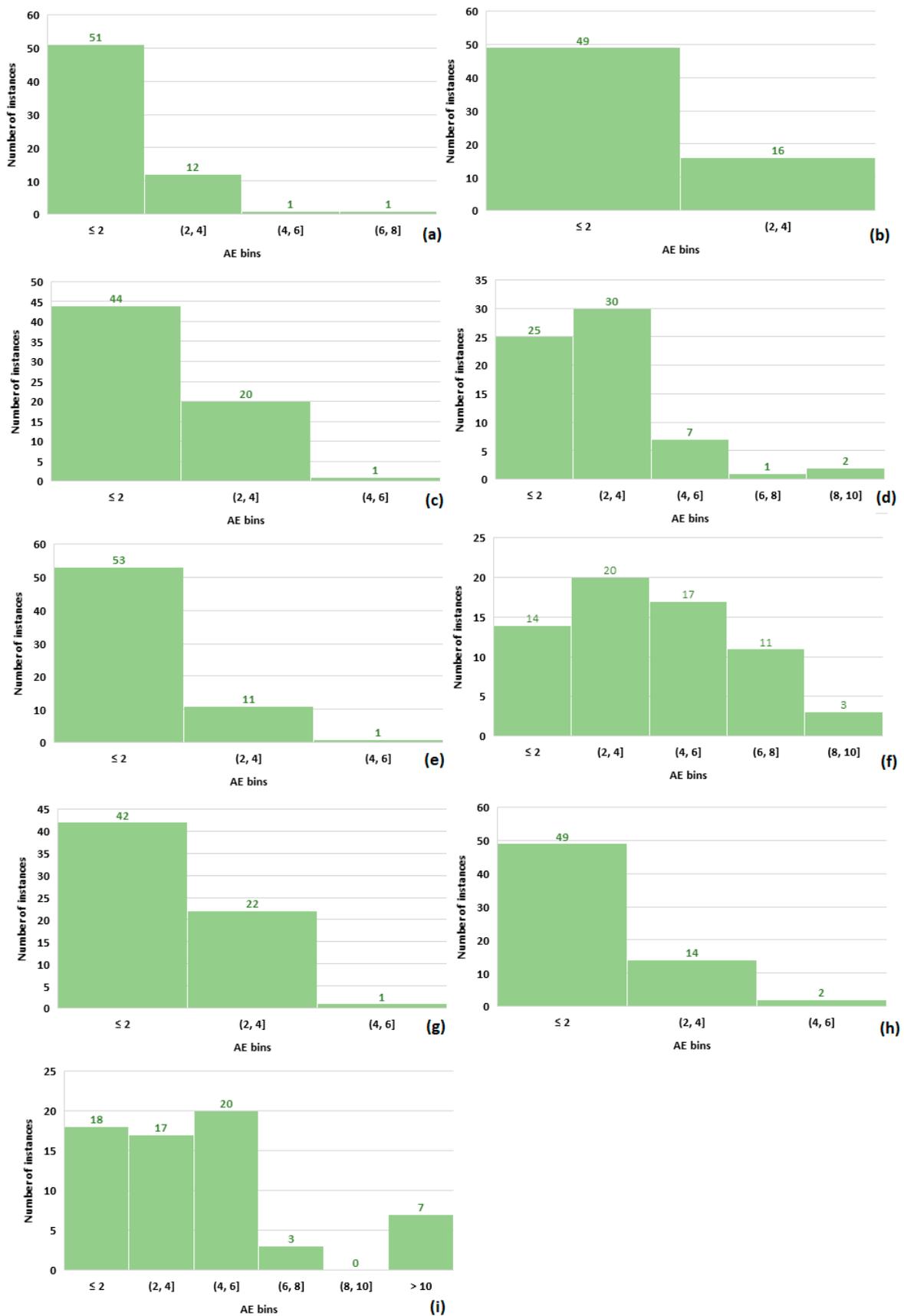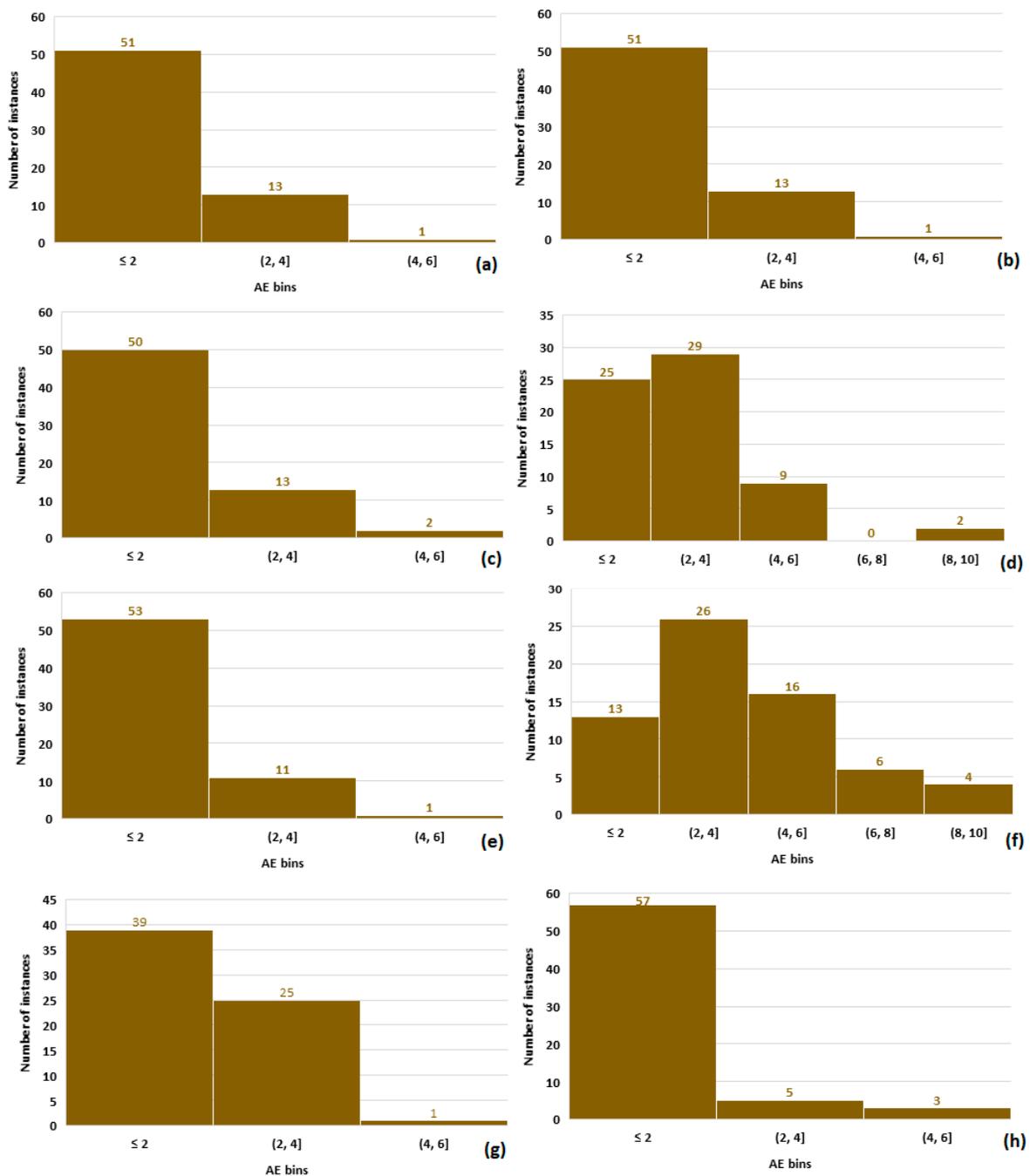
Figure 11. AE distribution for (**a**) ENN, (**b**) FFNN, (**c**) GMDH, (**d**) GRNN, (**e**) LSTM-ENN, (**f**) RBF, (**g**) RVM, (**h**) SVR, and (**i**) MRM for Test Case #2.

Figure 12. AE distribution for (**a**) ENN, (**b**) FFNN, (**c**) GMDH, (**d**) GRNN, (**e**) LSTM-ENN, (**f**) RBF, (**g**) RVM, and (**h**) SVR for Test Case #3.

The actual and the predicted time series for Test Case #1, Test Case #2, and Test Case #3 are shown in Figure 13, Figure 14, and Figure 15, respectively. It can be observed that predicted values of the proposed model are very close to the actual values and follow the same trend during the test process (65 observations). Large deviations are displayed by RBF and MRM. This fact confirms the corresponding values are high values of the error metrics. Moreover, robust models to predict the fuel demand at different conditions (wind, speed, main engine working hours, and LSFO fuel consumption) are the EN and FFNN due to the fact the fuel consumption displays a non-linear relationship with some of these variables, and these models better captured and simulated it.
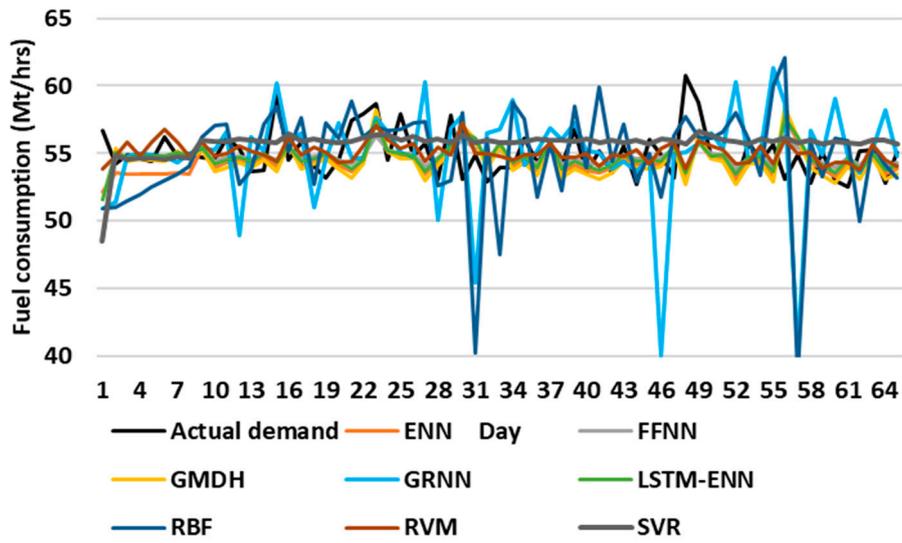
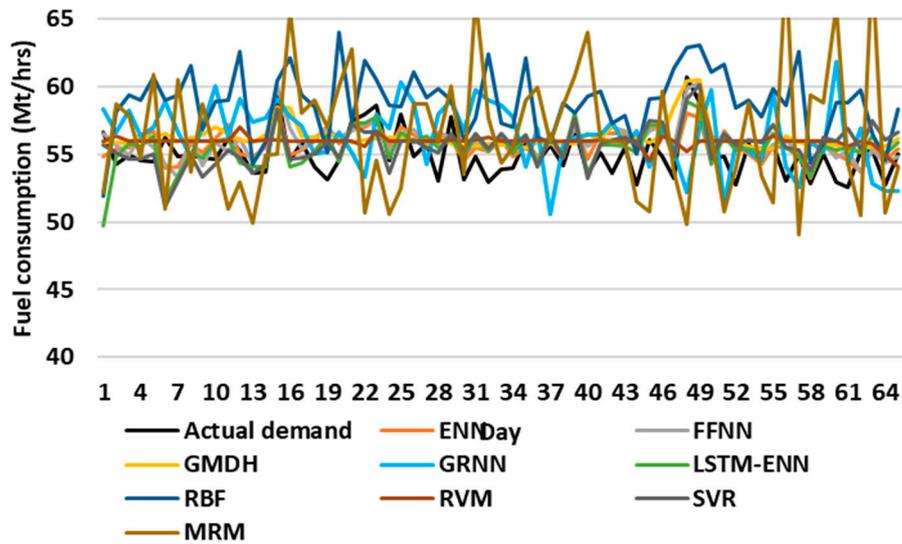**Figure 13.** Actual demand and forecasts for Test Case #1.

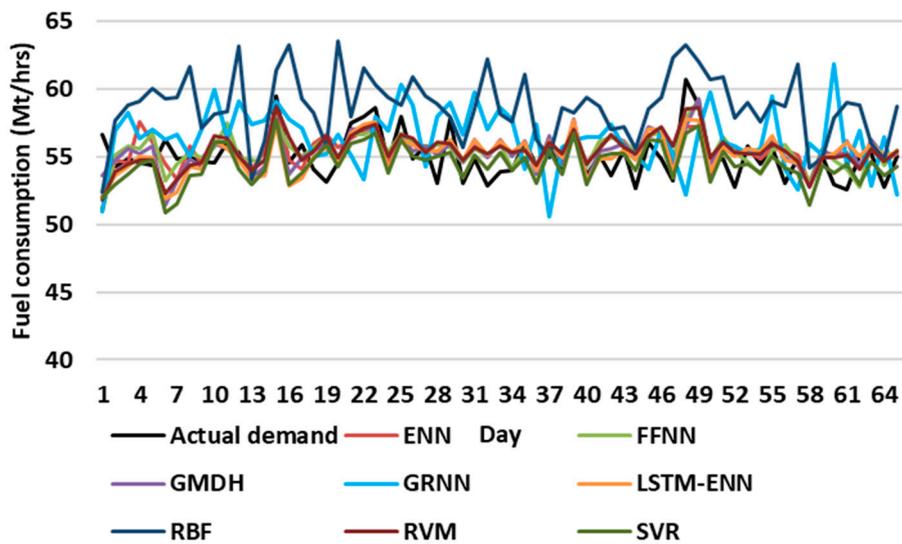**Figure 14.** Actual demand and forecasts for Test Case #2.

Figure 15. Actual demand and forecasts for Test Case #3.

5. Conclusions

An accurate fuel demand forecasting framework may lead to better management of ships' resources and to lower operational costs and emissions. While there is a lack in the literature of studies that are dedicated to predicting the fuel demand for passenger ships, the present paper is a first step towards studying the day-ahead forecasting problem. The aim of this study is two-fold: i) To present the variables on which the fuel consumption is dependent and ii) to present a forecasting model built on machine learning. It combines the two pillars of modern machine learning, i.e., shallow and deep learning. The model is compared with several machine learning and time series models.

The major findings of the paper reveal that a statistical analysis should precede model selection and training. For instance, and as is shown by the results of the paper, if a nonlinear relationship between fuel consumption and external variables is evident, models that are able to simulate this relationship are preferable. The ENN and the FFNN are the most preferable models after the proposed one. Although a neural network, RBF fails to provide accurate forecasts. This is due to its type of neuron activation function that is not suitable for the nonlinear relationship. An accurate prediction of the fuel demand, when based on accurate models, can significantly optimize the operational performance of a vessel. It is also taken into consideration that due to the fact that the voyage of a Ro/Pax vessel is predefined, by optimizing various parameters, a decrease in fuel consumption can be achieved.

References

1. DNV-GL. *Energy Transition Outlook 2017-Maritime Forecast to 2050*; Det Norske Veritas—Germanischer Lloyd: Oslo, Norway, 2017.
2. Notteboom, T. The impact of low sulphur fuel requirements in shipping on the competitiveness of roro shipping in Northern Europe. *WMU J. Marit. Aff.* **2010**, *10*, 63–95. [CrossRef]
3. Cruise Industry News. *Cruise Industry 2019 Financial Tracking*; Cruise Industry News: New York, NY, USA, 2019.
4. Kuriyama, A.; Abe, N. Ex-post assessment of the Kyoto Protocol—Quantification of CO_2 mitigation impact in both Annex B and non-Annex B countries. *Appl. Energy* **2018**, *220*, 286–295. [CrossRef]
5. European Commission. *Implementation of the Shipping MRV Regulation*; European Commission: Brussel, Belgium, 2017.
6. International Marine Organization. *Emission Control Areas (ECAs) Designated Under Regulation 13 of MARPOL Annex VI (NOx Emission Control)*; International Marine Organization: London, UK, 2018.
7. Nwaoha, T.; Ombor, G.; Okwu, M. A combined algorithm approach to fuel consumption rate analysis and prediction of sea-worthy diesel engine-powered marine vessels. *Proc. Inst. Mech. Eng. Part M J. Eng. Marit. Environ.* **2016**, *231*, 542–554. [CrossRef]
8. Castells Sanabra, M.; Usabiaga Santamaría, J.J.; Martínez De Osés, F.X. Manoeuvring and hotelling external costs: Enough for alternative energy sources? *Marit. Policy Manag.* **2013**, *41*, 42–60. [CrossRef]
9. Marine Insight. *What Is Nitrogen Oxides or NOx Air Pollution from Ships?* Marine Insight: Bangalore, India, 2017.
10. International Council on Clean Transportation. Air pollution and greenhouse gas emissions from ocean-going ships: Impacts, mitigation options and opportunities for managing growth. *Marit. Stud.* **2007**. [CrossRef]
11. Tzannatos, E.; Stournaras, L. EEDI analysis of Ro-Pax and passenger ships in Greece. *Marit. Policy Manag.* **2014**, *42*, 305–316. [CrossRef]
12. International Marine Organization. *Second IMO GHG Study 2009*; International Marine Organization: London, UK, 2009.
13. Talley, W. *The Blackwell Companion to Maritime Economics*; Wiley-Blackwell: Chichester, UK, 2012.

14. Beşikçi, B.E.; Arslan, O.; Turan, O.; Ölçer, A. An artificial neural network based decision support system for energy efficient ship operations. *Comp. Oper. Res.* **2016**, *66*, 393–401. [CrossRef]

15. Petersen, J.; Winther, O.; Jacobsen, D. A machine-learning approach to predict main energy consumption under realistic operational conditions. *Ship Tech. Res.* **2012**, *59*, 64–72. [CrossRef]

16. Pedersen, B.; Larsen, J. Prediction of full-scale propulsion power using artificial neural networks. In Proceedings of the 8th International Conference on Computer and IT Applications in the Maritime Industries (COMPIT '09), Budapest, Hungary, 10–12 May 2009; pp. 537–550.

17. Hochreiter, H.; Schmidhuber, J. Long short-term memory. *Neural Comp.* **1997**, *9*, 1735–1780. [CrossRef]

18. Meyer, J.; Stahlbock, R.; Voß, S. Slow steaming in container shipping. In Proceedings of the 45th Hawaii International Conference on System Sciences, Maui, HI, USA, 4–7 January 2012; pp. 1306–1314.

19. Cullinane, K. *International Handbook of Maritime Economics*; Edward Elgar: Cheltenham, UK, 2011.

20. Lundh, M.; Garcia-Gabin, W.; Tervo, K.; Lindkvist, R. Estimation and optimization of vessel fuel consumption. *IFAC PapersOnLine* **2016**, *49*, 394–399. [CrossRef]

21. Roh, M.; Lee, K. *Computational Ship Design*; Springer: Singapore, 2018.

22. International Organization for Standardization. *Requirements for Marine Distillate Fuels*; ISO 8217:2017; International Organization for Standardization: Geneva, Switzerland, 2017.

23. Nayak, N.; Lakshminarayanan, P. *Critical Component Wear in Heavy Duty Engines*; Wiley: Hoboken, NJ, USA, 2013.

24. Bomin. Heavy Fuel Oil. Available online: https://www.bomin.com/en/news-info/glossary/details/term/heavy-fuel-oil-hfo.html (accessed on 3 July 2019).

25. Weintrit, A.; Neuman, T. *Marine Navigation and Safety of Sea Transportation*; Taylor and Francis: Boca Raton, FL, USA, 2013.

26. Acomi, N.; Acomi, O. The influence of different types of marine fuel over the energy efficiency operational index. *Energy Proc.* **2014**, *59*, 243–248. [CrossRef]

27. Koffi, B.; Cerutti, A.; Duerr, M.; Iancu, A.; Kona, A.; Janssens-Maenhout, G. CoM Default Emission Factors for the Member States of the European Union 2017. Available online: https://data.europa.eu/euodp/en/data/dataset/jrc-com-ef-comw-ef-2017 (accessed on 3 July 2019).

28. Fagerholt, K.; Laporte, G.; Norstad, I. Reducing fuel emissions by optimizing speed on shipping routes. *J. Oper. Res. Soc.* **2010**, *61*, 523–529. [CrossRef]

29. Lu, R.; Turan, O.; Boulougouris, E. Voyage optimization: Prediction of ship specific fuel consumption for energy efficient shipping. In Proceedings of the 3rd International Conference on Technologies, Operations, Logistics and Modelling for Low Carbon Shipping, London, UK, 9–11 September 2013; pp. 1–11.

30. Foundation for Economic & Industrial Research. *The Contribution of Coastal Shipping to the Greek Economy: Performance and Outlook*; Foundation for Economic & Industrial Research: Athens, Greece, 2014.

31. Eurostat. *Country Level—Passengers Embarked and Disembarked in All Ports, by Direction*; Eurostat: Luxembourg, 2018.

32. Marine Insight. What are Ro-Ro Ships? Available online: https://www.marineinsight.com/types-of-ships/what-are-ro-ro-ships (accessed on 3 July 2019).

33. Saraçoğlu, H.; Deniz, C.; Kılıç, A. An investigation on the effects of ship sourced emissions in Izmir port, Turkey. *Sci. World J.* **2013**, *2013*, 1–8. [CrossRef] [PubMed]

34. Pacetti, M. *The Sustainable City VII*; WIT Press: Southampton, UK, 2012.

35. Xu, R.; Wunsch, D. *Clustering*; John Wiley & Sons. Inc.: Hoboken, NJ, USA, 2006.

36. Gusti, A.; Semin, S. The effect of vessel speed on fuel consumption and exhaust gas emissions. *Am. J. Eng. Appl. Sci.* **2016**, *9*, 1046–1053. [CrossRef]

37. International Marine Organization. *Energy Efficiency Measures*; International Marine Organization: London, UK, 2018.

38. Zheng, J.; Xu, C.; Zhang, Z.; Li, X. Electric load forecasting in smart grid using long-short-term-memory based recurrent neural network. In Proceedings of the 51st Annual Conference on Information Sciences and Systems, Baltimore, MD, USA, 22–24 March 2017; pp. 1–6.

39. Wang, H.; Yi, H.; Peng, J.; Wang, G.; Liu, Y.; Jiang, H.; Liu, W. Deterministic and probabilistic forecasting of photovoltaic power based on deep convolutional neural network. *Energy Conv. Manag.* **2017**, *153*, 409–422. [CrossRef]

40. Soldo, B.; Potocnik, P.; Simunovi Sari, G.T.; Govekar, E. Improving the residential natural gas consumption forecasting models by using solar radiation. *Energy Build.* **2014**, *69*, 498–506. [CrossRef]

41. Xu, F.Y.; Leung, M.C.; Zhou, L. A RBF network for short-term load forecast on microgrid. In Proceedings of the 2010 International Conference on Machine Learning and Cybernetics, Qingdao, China, 11–14 July 2010; pp. 1–3.

42. Nose-Filho, K.; Plasencia Lotufo, A.D.; Minussi, C.R. Short-term multinodal load forecasting using a modified general regression neural network. *IEEE Trans. Power Del.* **2011**, *26*, 2862–2869. [CrossRef]

43. Liu, B. Short-term load forecasting of distributed energy supply system based on Elman neural network. In Proceedings of the 2018 China International Conference on Electricity Distribution, Ljubljana, Slovenia, 17–19 September 2018; pp. 2175–2178.

44. Zhang, M.G. Short-term load forecasting based on support vector machines regression. In Proceedings of the 2005 International Conference on Machine Learning and Cybernetics, Guangzhou, China, 18–21 August 2005; pp. 4310–4314.

45. Abdel-Aal, R.E.; Elhadidy, M.A.; Shaahid, S.M. Modeling and forecasting the mean hourly wind speed time series using GMDH-based abductive networks. *Renew. Energy* **2009**, *34*, 1686–1699. [CrossRef]

46. Sun, G.; Chen, Y.; Wei, Z.; Li, X.; Cheung, K.W. Day-ahead wind speed forecasting using relevance vector machine. *J. Appl. Math.* **2014**, *2014*, 1–6. [CrossRef]

47. Kizilaslan, R.; Karlik, B. Comparison neural networks models for short term forecasting of natural gas consumption in Istanbul. In Proceedings of the International Conference on the Applications of Digital Information and Web Technologies 2008, Ostrava, Czech Republic, 4–6 August 2008; pp. 448–453.

48. Keith, T. *Multiple Regression and Beyond: An Introduction to Multiple Regression and Structural Equation Modeling*; Routledge: New York, NY, USA, 2015.

49. Osborne, J.; Waters, E. Four assumptions of multiple regression that researchers should always test. *Pract. Assess. Res. Eval.* **2002**, *8*, 1–5.

50. Górski, W.; Abramowicz-Gerigk, T.; Burciu, Z. The influence of ship operational parameters on fuel consumption. *Zeszyty Naukowe* **2013**, *36*, 48–54.

51. MacKay, D.J.C. Bayesian interpolation. *Neural Comp.* **1992**, *4*, 415–447. [CrossRef]